Supplemental figures

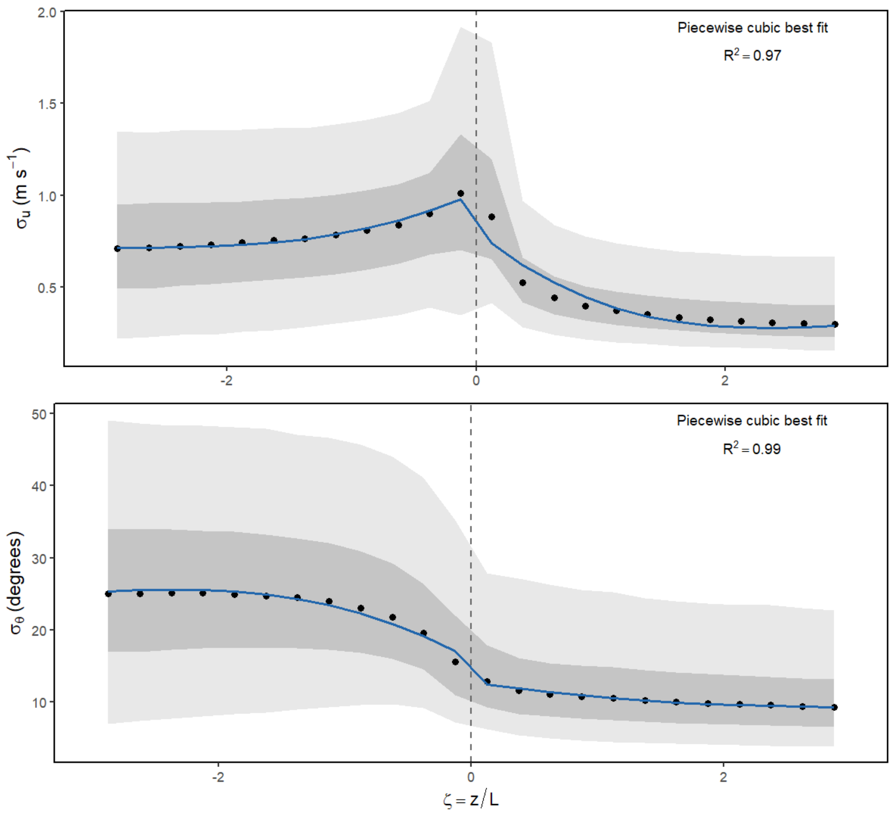

Figure S1. AmeriFlux-derived wind variability as a function of Monin-Obukhov stability, expressed as ζ = z/L. Points show binned medians across 8,547,333 retained half-hourly or hourly observations from 173 AmeriFlux sites. Shaded regions show the interquartile range and 5th-95th percentile envelope within each stability bin. The blue line is the best-fit piecewise cubic relationship used to parameterize stability-dependent wind variability, with σ_u fit performance of R^2 = 0.974, and σ_θ fit performance of R^2 = 0.995.

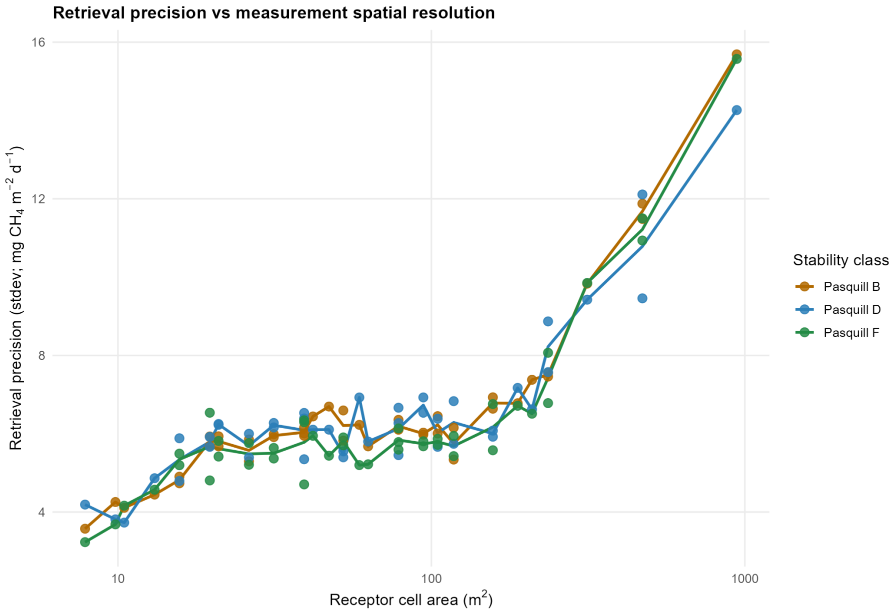

Figure S2. Retrieval precision as a function of receptor cell area under constant atmospheric forcing. Points show the retrieval standard deviation for individual azimuth-height sampling configurations, and lines show the mean precision at each receptor cell area for each Pasquill stability class. Precision is reported as the standard deviation of retrieved methane flux across 100 replicates for a 100 m diameter lake emitting 50 $\mathrm{mg\,CH_4\,m^{-2}\,d^{-1}}$.

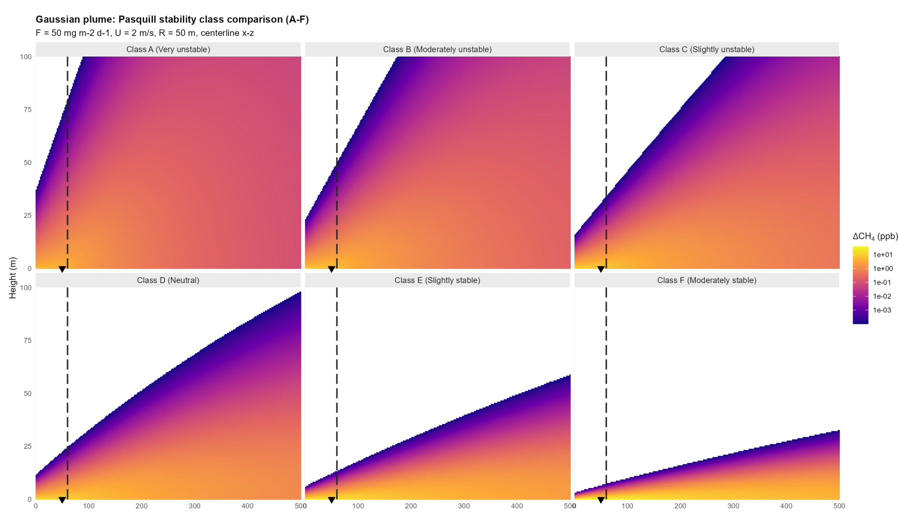

Figure S3. Centerline Gaussian plume cross-sections for a 100 m diameter lake emitting methane at 50 $\mathrm{mg\,CH_4\,m^{-2}\,d^{-1}}$ under a 2 $\mathrm{m\,s^{-1}}$ wind. Panels compare Pasquill stability classes A-F using the same logarithmic color scale for methane enhancement. The black marker denotes the downwind lake boundary, and the dashed vertical line marks the nominal downwind receptor plane 10 m beyond the shoreline. Increasing atmospheric stability confines vertical dispersion, producing a shallower, more persistent near-surface plume downwind.

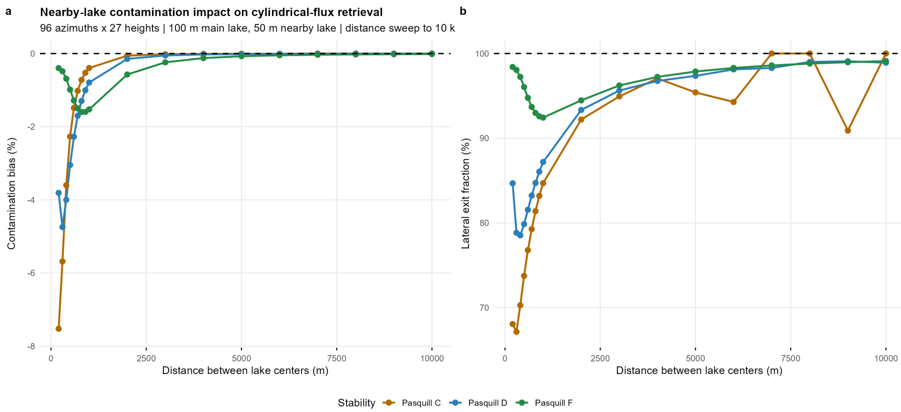

Figure S4. Distance decay of nearby-lake contamination bias over a 10 km separation sweep from Experiment 2. Mean contamination bias (a) and lateral exit fraction (b) are shown for a 50 m diameter upwind nearby lake placed 200 m to 10,000 m from a 100 m diameter target lake. Curves compare Pasquill C, D, and F stability classes; points are means and ribbons are $\pm$ 1 standard deviation across 100 repetitions.

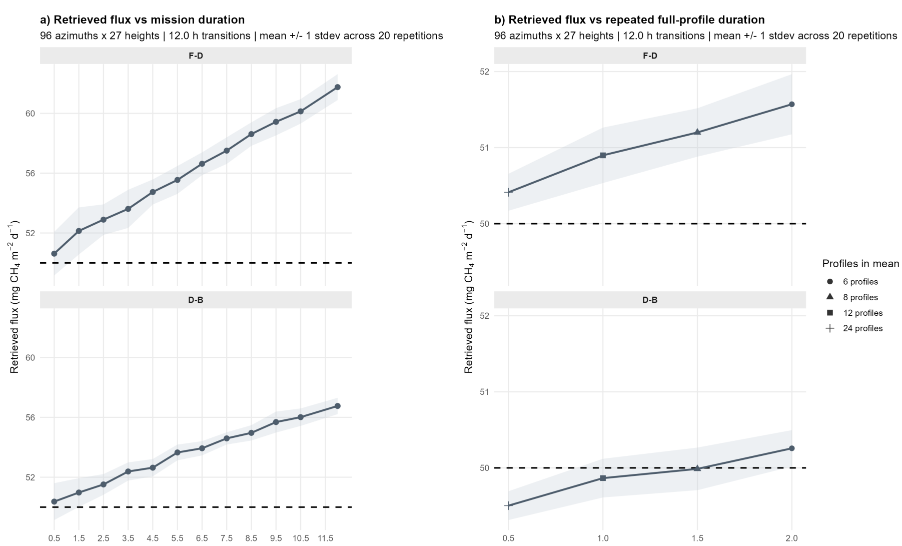

Figure S5. Retrieved $\mathrm{CH_4}$ flux is shown for the F–D and D–B stability transitions under two sampling strategies: (a) single sequential missions from 0.5 to 12 h, and (b) repeated full-profile measurements with 0.5 to 2 h per profile averaged over the 12 h transition window. Lines show means, ribbons show $\pm$ 1 standard deviation across 20 repetitions, and the dashed line marks the true flux of 50 $\mathrm{mg\,CH_4\,m^{-2}\,d^{-1}}$.

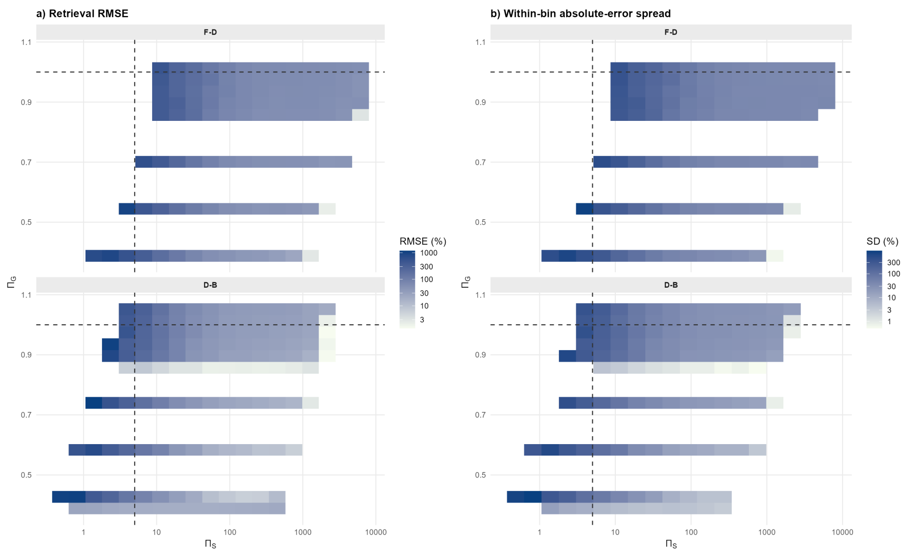

Figure S6. Dimensionless retrieval-error framework for the atmosphere stability transition cases. Rows show F–D and D–B atmospheric stability transitions. The left column (a) shows flux-retrieval RMSE, expressed as percent error relative to the prescribed lake-mean flux, binned in 20 bines each for Π_S and Π_G. The right column shows the within-bin spread in standard deviation of RMSE for bins with at least five values. The vertical dashed line marks $\Pi_S = 5$, a practical low-detectability reference, and the horizontal dashed line marks $\Pi_G = 1$, the theoretical transition where lateral signal extent is comparable to the control-volume radius. RMSE is presented in logarithmic scale and standard deviation of RMSE in linear scale.